CCFE
CULHAM CENTRE FOR FUSION ENERGY

UK Atomic Energy Authority

UKAEA-CCFE-PR(22)48

N. VIANELLO, N. WALKDEN, M. DUNNE, B. LOMANOWSKI, E. WOLFRUM, C. TSUI, A. STAGNI, M. GRIENER, B. TAL, T. EICH, D. REFY, D. BRIDA, O. FEVRIER, M. AGOSTINI, H. DE OLIVEIRA, S. ALEIFERIS, M. BERNERT, J. BOEDO, et al

SOL PROFILE AND FLUCTUATIONS IN DIFFERENT DIVERTOR RECYCLING CONDITIONS IN H-MODE PLASMAS

SOL PROFILE AND FLUCTUATIONS IN DIFFERENT DIVERTOR RECYCLING CONDITIONS IN H-MODE PLASMAS

N. VIANELLO, N. WALKDEN, M. DUNNE, B. LOMANOWSKI, E. WOLFRUM, C. TSUI, A. STAGNI, M. GRIENER, B. TAL, T. EICH, D. REFY, D. BRIDA, O. FEVRIER, M. AGOSTINI, H. DE OLIVEIRA, S. ALEIFERIS, M. BERNERT, J. BOEDO, et al

This is a preprint of a paper submitted for publication in Nuclear Fusion

SOL PROFILE AND FLUCTUATIONS IN DIFFERENT DIVERTOR RECYCLING CONDITIONS IN H-MODE PLASMAS

N. VIANELLO[1], N. WALKDEN[2], M. DUNNE[3], B. LOMANOWSKI[4], E. WOLFRUM[3], C. TSUI[5], A. STAGNI[1], M. GRIENER[3], B. TAL[3], T. EICH[3], D. REFY[6], D. BRIDA[3], O. FÈVRIER[7], M. AGOSTINI[1], H. DE OLIVEIRA[7], S. ALEIFERIS[8], M. BERNERT[3], J. BOEDO[5], M. BRIX[2], D. CARRALERO[9], I. CARVALHO[2], L. FRASSINETTI[10], C. GIROUD[2], A. HAKOLA[1], A. HUBER[11], J. KARHUNEN[13], A. KARPUSHOV[7], B. LABIT[7], A. MEIGS[2], V. NAULIN[14], T. PEREIRA[15], C. PEREZ VON THUN[16], H. REIMERDES[7], C. THEILER[7], the ASDEX-Upgrade Team[*], the TCV team[**], the EUROfusion MST1 Team[***] and and the JET Contributors[****]

[1] [1]*Consorzio RFX, Padova,Italy,* [2]*CCFE, Culham, UK,* [3]*Max-Planck-Institut für Plasmaphysik, Garching, Germany,* [4]*Oak Ridge National Laboratory, Oak Ridge, USA* [5]*UCSD, La Jolla, USA,* [6]*Centre for Energy Research, Hungary,* [7]*EPFL-SPC, Switzerland,* [8]*NCSR Athens GR,* [9]*CIEMAT Laboratorio Nacional de Fusión, Madrid, Spain,* [10]*Division of Fusion Plasma Physics, KTH, Stockholm SE,* [11]*VTT, Espoo, Finland,* [12]*Forschungszentrum Julich,* [13]*Aalto University, Espoo, Finland,* [14]*DTU, Copenhagen, Denmark,* [15]*IST/IPFN, Lisbon, Portugal* [16]*IPPLM, Warsaw, Poland* [*] *See author list in H. Meyer et al, 2019, Nucl. Fusion 59 112014* [**] *See author list of S. Coda et al 2019 Nucl. Fusion 59 112023* [***] *See the author list B. Labit et al 2019 Nucl. Fusion 59 086020,* [****] *See the authors list E. Joffrin et al 2019 Nucl. Fusion 59 112021*

Corresponding Author: nicola.vianello@igi.cnr.it

Abstract:

The evolution of SOL density profiles and fluctuations have been studied at different recycling levels in 3 different tokamaks, ASDEX-Upgrade, TCV and JET, all operated in H-Mode. In all devices we clearly observe an increase of far SOL e-folding length at high fuelling with the divertor at least in high-recycling regime and high divertor neutral pressure. The observed variation is generally associated to an increase filamentary activity with indication of faster more frequent filaments in the far SOL. The relation of SOL turbulence with divertor and separatrix conditions will be discussed.

1 INTRODUCTION

Plasma Wall Interaction (PWI) is a subject of intense study in the context of fusion energy research for the understanding of the amount of heat loads, tritium retention, and the lifetime of different Plasma Facing Components. In order to ensure reliable predictive edge modeling it is mandatory to determine the transport properties of the Scrape Off Layer (SOL), a region largely influenced by the presence of turbulent filaments which contribute to particle and energy losses in both L and H modes. From the ITER divertor perspective, to keep the power fluxes acceptable for target material, high neutral pressure and partial detachment are needed to ensure maximum tolerable loads and avoid W recrystallization, conditions which presently set the upper limit of acceptable power fluxes [1]. All these requests motivated an experimental investigation of edge transport in conditions mimicking ITER conditions, and in particular on the upstream SOL modifications caused by increase neutral pressure and increase dissipation in the divertor. Among all the physical process evolving whenever changing the fueling level, this contribution will concentrate on the process of SOL density profile broadening also known as *shoulder formation*. In L-Mode, this process describes the progressive flattening of the SOL density profile whenever the core density is increased [2–6] This is generally associated to an increase of the convective component of the radial transport which could pose serious problems for first wall Plasma Facing Components. This contribution will investigate H-Mode plasmas extending previous investigations [7–13] which already suggested that similar inter-ELM SOL density profile broadening is observed in H-mode with a stronger dependence on the neutral pressure. The manuscript will report on the observed increase of filamentary activity associated to these high density regimes, which often are observed to move to a different pedestal stability region where the so-called *small ELMs* [14] or *Quasi continuous exhaust* (QCE) [12] dominate. We will also try to relate the observed SOL transport changes to the balloning paradigm suggested as possible explanation of the H-mode density limit [15, 16]. The experimental activity has been carried out on 3 different devices, JET, ASDEX-Upgrade (AUG) and TCV, thus providing an exploration in a wide operational space, from a device with a closed divertor, metallic first wall and cryogenic pumping system to a carbon machine, which even with recently included baffles [17] exhibits a much lower divertor closure.

2 ASDEX-UPGRADE

On ASDEX-Upgrade different scenarios have been explored where both fueling and NBI heating have been varied spanning a range in power linear density $P/R \simeq 1-7$ MW/R. All the investigation exploited the so-called *Edge Optimized Shape* (EOC) configuration with an uppder triangularity $\delta_u = 0.1$ and a plasma boundary conforming to the outer protection limiter. The typical waveforms of main plasma parameters for one of this discharge at I_p = 0.8MA, B_t=2.4T with a total additional power of 6.2MW from a combination of NBI and ECRH are shown in Fig. 1.

As we can clearly see the discharge exhibits a continuous increase of the edge density and corresponding divertor and midplane neutral pressure. The first observation is the strong reduction of ELM activity which can be noted

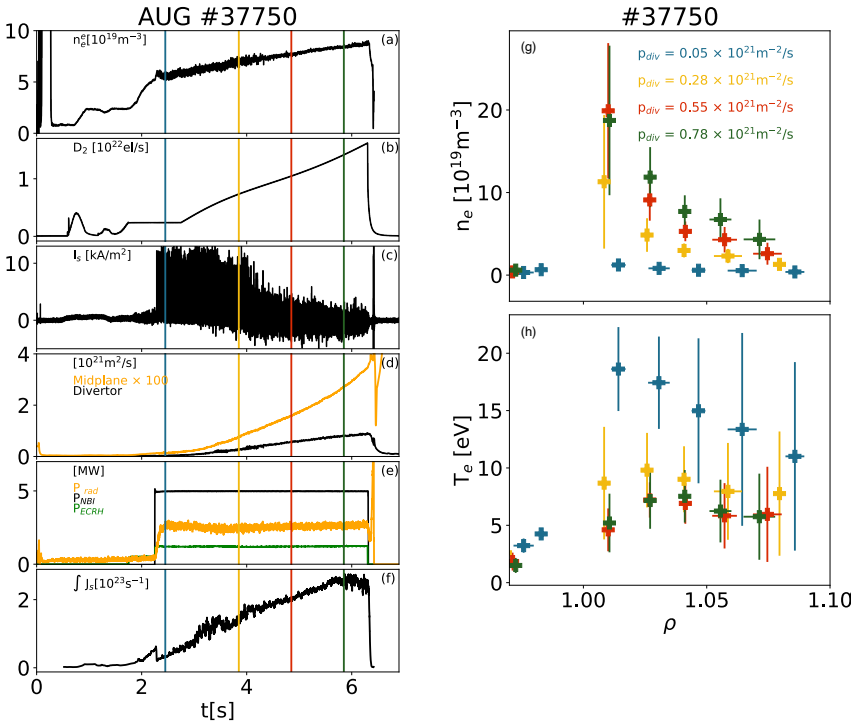

FIG. 1: (a) Line average density from edge interferometer chord (b) Total gas fuelling (c) Divertor shunt current, used for ELM-monitoring (d) Divertor and midplane neutral pressure multiplied by a factor of 100 from fast gauges (e) NBI, ECRH and total radiation power (f) Total integrated ion flux to the outer target from langmuir probes (g) Target density profiles from divertor langmuir probes at different time istants. Color codes refer to the vertical lines in panels (a-f) (h) Target temperature profiles from divertor langmuir probes at different time istants

from approximately 4 s. Indeed the divertor shunt current (panel (c) of Fig. 1), generally used as ELM monitoring at AUG, exhibit a strong reduction in amplitude from 4 s and no clear signature of ELMs can be seen anymore. This is a know feature indicating the transition to the small-ELM regimes [14] recently named as *Quasi Continuous Exhaust* (QCE) regime [12]. The total ion flux does not exhibit signature of roll-over, with just a small inflection around 6 seconds suggesting that the outer divertor is still in high-recycling regime throughout the entire discharge. This can be confirmed as well from panels (g) and (h) of figure 1 where the inter-ELM density and temperature profiles as derived from embedded langmuir probes are shown. Outer Strike Point (OSP) temperature reduces to values close to 5 eV but at the same time target density is still increasing thus confirming the plasma is still in high-recycling. It is worth noting that whenever the discharge moves into small-ELM, the distinction between ELM and no-ELM activity can't be performed anymore and thus the profiles are obtained from the entire signal.

It is already well known that increasing fueling causes a modification of the upstream pedestal and Scrape Off layer profile. For a proper determination of the separatrix position we apply the same methodology described in [15]: the separatrix temperature $T_{e,sep}$ is computed as:

$$T_{e,sep} \approx \left(\frac{7}{16} \frac{P_{sep} q_{cyl}^2 A}{\kappa_0^e \hat{\kappa} \langle \lambda_q \rangle} \right)^{\frac{2}{7}} \tag{1}$$

with $A = R/a$ the aspect ration, κ_0^e the electron heat condution, $\hat{\kappa} = \left(\frac{1+\kappa_{geo}}{2} \right)^{0.5}$, $q_{cyl} = \frac{B_{tor}}{\langle B_{pol} \rangle} \cdot \frac{\hat{\kappa}}{A}$, $\langle B_{pol} \rangle = \frac{\mu_0 I_p}{2\pi a \hat{k}}$. This procedure allows a better estimate of the separatrix temperature and density. From panel (a) of 2 we recognize that $n_{e,sep}$ exhibits a strong correlation with divertor neutral pressure as already reported in [18, 19]. The knowledge of separatrix condition allows as well an evaluation of the the normalized collisionality α_t introduced in [15]:

$$\alpha_t = 3 \times 10^{-18} R q_{cyl}^2 \frac{n_e}{T_e^2} Z_{eff} \tag{2}$$

which describes the relative effect of the interchange drive on the drift-wave and it is closely related to the diamagnetic parameter α_d introduced in [20]. The same panel (a) of figure 2 shows as well the almost linear dependence between the turbulence parameter α_t and the divertor pressure through the observed scaling of the separatrix density in line with the observation in [15]. The inter-ELM density profiles at different divertor pressure levels are reported in Figure 2 (b): we observe clearly an increase of the pedestal top density and as well of the separatrix density with a corresponding decrease of the maximum density gradient in the pedestal region. The modification of the SOL

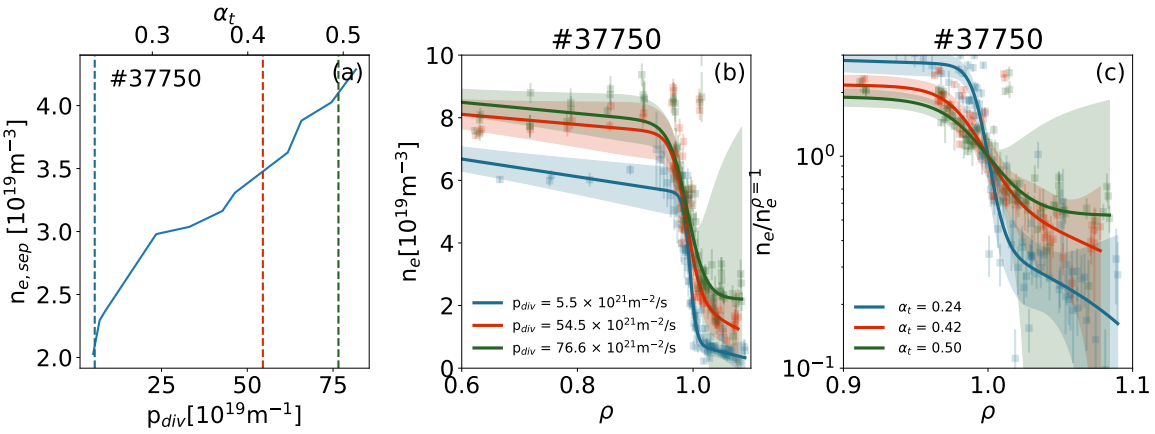

FIG. 2: (a) Separatrix density $n_{e,sep}$ as a function of divertor neutral pressure and ballooning turbulence parameter α_t. (b) Upstream profile at different values of divertor neutral pressure. The solid line is the result of a mtanh fit whereas the shaded region indicate the 3σ error estimate on the fit. (c) Upstream profiles normalized to the value at the separatrix at different values of ballooning parameter α_t

density profile can be better appreciated in panel (c) of the same figure 2 where the profiles are shown as normalized to the separatrix condition. A pronounced density shoulder forms whenever we move to higher divertor pressure levels or equivalently at higher turbulence parameter α_t. To quantify the evolution of the profile broadening we compute the density e-folding length $\lambda_n = \mid n_e/\nabla n_e \mid$ still as a function of α_t and divertor pressure as shown in 3. A clear increase of the density e-folding length is observed with values which are almost doubling whenever

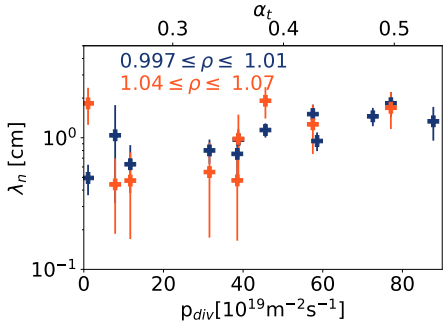

FIG. 3: Scaling far density e-folding length as a function of p_{div} and α_t

pressure and correspondingly α_t is increasing suggesting a strong link between far SOL density and corresponding turbulence strength at the separatrix.

For L-Mode studies the role of enhanced convective filamentary transport in the formation of SOL density shoulder has been already reported several times [3, 4, 11]. A clear proportionality between blob-size and SOL e-folding length has been clearly confirmed in both AUG and TCV [11] with a strong relation with the detachment status. On the other side, the paradigm observed in L-Mode does not hold strictly in H-Mode, where dissipative divertor achieved by strong extrinsic impurity seeding with low fuelling does not cause any modification of the upstream profiles [21]. As well the same relation between blob-size and e-folding length is not as robust as the L-mode cases. For this reason an extensive analysis has been performed using the Thermal Helium Beam diagnostic [22], which is able to provide high spatial and temporally resolved measurements of Helium light emission from a locally puffed helium cloud. The collected light emission is thus proportional to local density and it can be used to infer the local velocity of the SOL propagating filaments. The analysis of this signal for the same shot reported in figure 1 is shown in Fig 4

The first important information is the increase of the filament frequency as a function of divertor neutral pressure or equivalently with the turbulent parameters α_t. This observation has been already reported in [12] and confirms that whenever the α_t parameter increases, a stronger ballooning dominated turbulence activity is observed close to the separatrix, and this contributes to a larger number of filaments expelled into the SOL region. In panel (b) of the same Fig 4 we also compute the histogram of filament radial velocity at the same radial location. We clearly observe that whenever the turbulent parameter α_t increases there is an increase of the population of filaments with higher radial velocity $v_r \approx 1$ km/s which is completely absent at lower p_{div} or lower α_t. The mechanism of shoulder formation in H-Mode appears thus strongly related to changes of the turbulence close to the separatrix: this is related to the increase of the ballooning turbulence at the separatrix achieved through modification of separatrix density caused by the strong divertor pressure achieved. With the increase of α_t the SOL start to be filled with more filaments with a larger average velocity thus increasing the convective component of the radial transport.

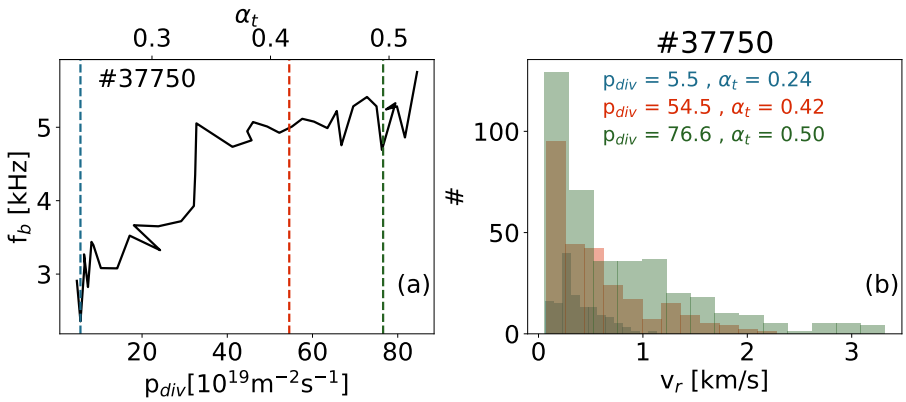

FIG. 4: (a) Filament frequency at $\rho \approx 1.07$ as a function of divertor pressure and α_t (b) Histogram of filament radial velocity at $\rho \approx 1.07$ at different values of p_{div} and α_t. The color codes correspond to the vertical lines in panel (a)

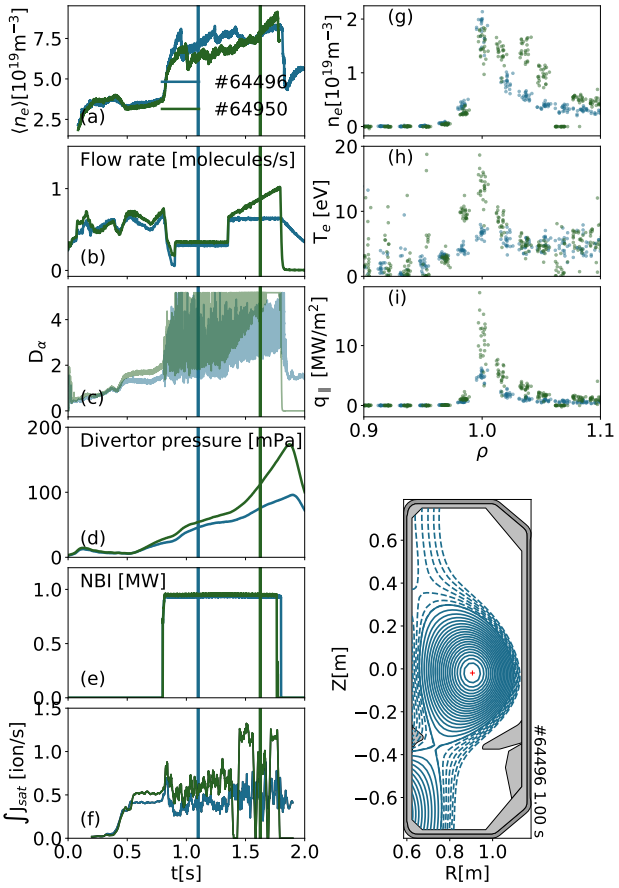

FIG. 5: (a) Line average density from a peripherical chord (b) Divertor gas fuelling (c) D_α from a vertical LoS (d) Divertor neutral pressure (e) NBH heating power (f) Total integrated ion flux at the Outer Target (g) Inter-ELM Outer target density profiles at two different time intervals indicated by vertical lines in panels (a-f) (h) Inter-ELM Outer target temperature profiles (i) Inter-ELM Outer target parallel heat flux

3 TCV

On TCV an NBH heated H-mode plasma scenario has been investigated with different values of divertor fuelling controlled in feed-forward. Even though the investigation has been carried out both in baffled and unbaffled scenarios, only operation with installed baffles will be considered in this contribution, leaving the comparison with a complete open divertor to further investigation. The plasma shape features a very high upper triangularity $\delta_u \approx 0.4$ with the secondary X-point sitting inside the vessel. Several discharges were performed, while keeping the same shape and power and changing only the fueling waveforms. Two examples of such discharges are shown in Figure 5 They exhibit the same 1 MW heating power and up to 1.2 s the same fuelling waveform: after that an additional fuelling ramp is applied to shot 64950, reaching higher neutral pressure while no significant increase of the line average density from the edge interferometer chord can be observed (panel (a) of Fig.5). The ELM behavior, as

monitored by the D_α signal from vertical Line of Sight, exhibits a modification in the higher fuelling case moving towards small-ELM regimes. From the total integrated ion-flux shown in panel (f) no indication of achieved detachment or rollover is observed. In panel (g)-(i) the inter-ELM target profiles as deduced from embedded langmuir probes are shown for the two shots in different time instants indicated by colored vertical lines in panels (a)-(f). The Outer Strike Point (OSP) temperature is well above 10 eV for both the cases whereas target density seems to broaden at higher neutral pressure. For completeness in panel (i) we also show the parallel heat flux deduced from langmuir probes as [23]$q_{||} = en_e^t c_s(\gamma T_e + E_{pot})$ with $c_s = \sqrt{(T_e + T_i)/m_i}$ where $T_e = T_i$ assumption is made, the heat transmission function is assumed to be $\gamma = 5$ and the $E_{pot} = (13.6 + 2.2)$ eV is the potential energy carried by each outgoing ion, including the hydrogen ionization energy and half of the molecular binding energy. The evaluation of the $q_{||}$ profile is used to infer the corresponding λ_q and consequently the separatrix temperature still according to Eq. (1). Given the corresponding value of the separatrix density we can as well deduce the variation of the already introduced turbulent parameter α_t. It is worth mentioning that the evaluation of α_t for TCV suffers from the lack of precise determination of Z_{eff} at the separatrix. Our best estimate sets a value of $Z_{eff} \simeq 1.9 \pm 0.4$. The evaluation of $n_{e,sep}$ and α_t using all the available database is shown in Figure 6 As for the

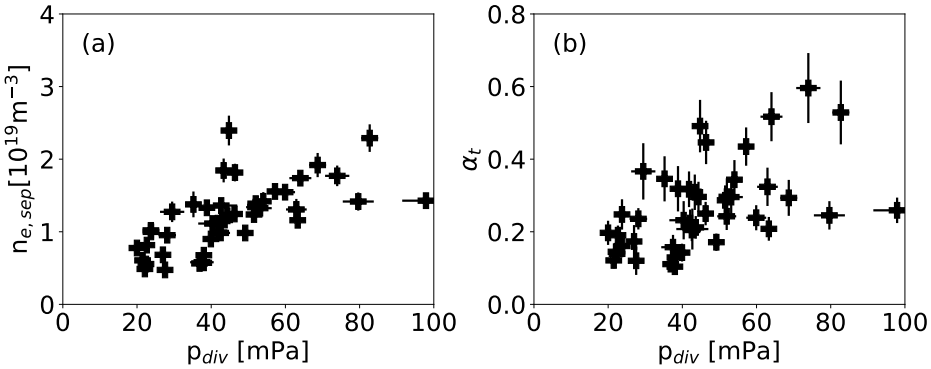

FIG. 6: (a) Separatrix density as a function of divertor neutral pressure (b) α_t as a function of divertor neutral pressure

case of AUG, separatrix density is found to increase with divertor neutral pressure as seen in panel (a). This implies as well a modification of the α_t values which still exhibit an increasing trend with p_{div} suggesting that in the scenarios at higher neutral pressure and separatrix density ballooning like turbulence become much more important. The evolution of upstream density profile is shown in figure 7 The profiles are shifted in order to match the estimated

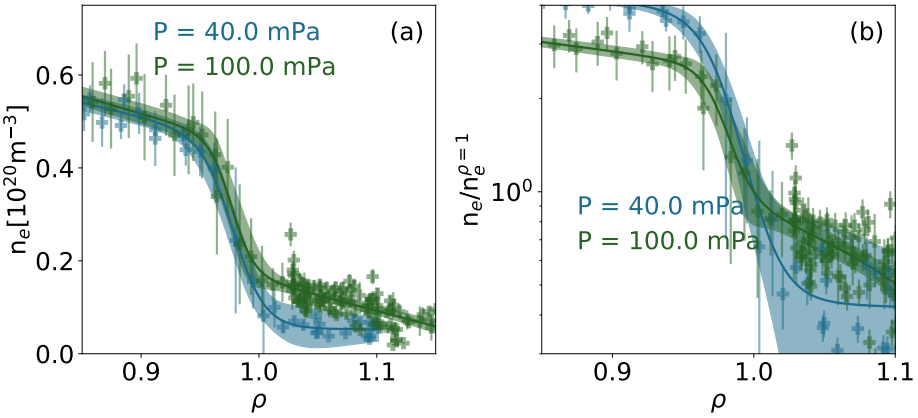

FIG. 7: (a) Upstream density profile at two different values of divertor neutral pressure (b) Upstream density profiles normalized to the value at the separatrix. The solid line represents a modified tanh fit whereas the shaed area a propagation of the 3σ error on the fit parameter

separatrix value as described in previous section: whenever a clear identification of the ELM from D_α monitor was possible, in the case at lower pressure, we evaluate the inter-ELM profiles within 70-90 % of the ELM cycle. We clearly observe that differently from what observed on AUG the increase of the pressure lead to a significant increase of the separatrix density but not of the top-pedestal one: but more clearly the two scenarios exhibit a rather different SOL density with a clear shoulder building up whenever higher neutral pressure, or equivalently higher α_t is achieved. Finally in order to check if the flatter SOL profile is associated with a corresponding increase of

the far SOL turbulence we evaluate the frequency of filaments f_b detected from wall embedded langmuir probes, operated in constant biased mode to obtain highly temporally resolved measurements of the ion saturation current J_s. The results of the analysis is shown in Figure 8 The blobs are evaluated only in the inter-ELM region and are

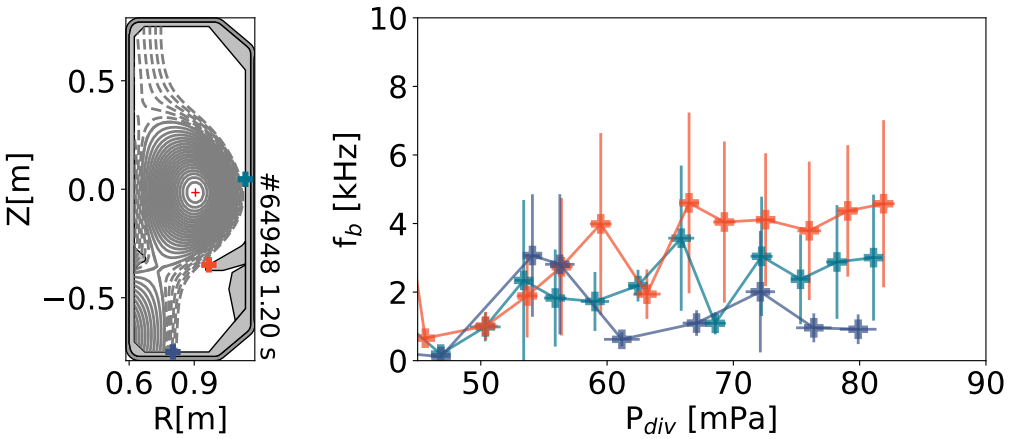

FIG. 8: Blob frequency as a function of divertor neutral pressure as inferred from embedded langmuir probes. The color codes refer to different probes in different poloidal regions: the corresponding positions is shown in the left hand poloidal cross-section of TCV device

detected using the signal normalized by subtracting a running mean and dividing by a running standard deviation with a windowing of 5 ms to take into account possible secular increase due to the higher density explored during the discharges. Evolution of f_b in 3 different poloidal locations are shown, with the corresponding positions shown in the machine cross section in Fig. 8. We clearly observe that both the probe sitting in the outer wall and the one sitting on the baffle nose exhibit an increase of the detected blob whereas no large variation is seen at the target. The analysis is thus consistent with the observations on AUG shown in figure 4 (a) and confirms the increase blob frequency in the far SOL whenever higher separatrix α_t is achieved by increasing fuelling.

4 JET

On JET a series of discharges with I_p=2MA, B_t =2.3 T in low-δ configuration with a total heating power of approximately 19 MW (16MW of NBI, 2-3 MW ICRH) have been performed. In this series of discharges different levels of fuelling have been explored, by keeping the fuelling locations in the same locations. The experiments aimed to investigate the effect of different divertor geometries in setting separatrix, upstream SOL and pedestal conditions, motivated by already suggested experimental observations reported in [24, 25] according to which clear differences in global confinement as well in pedestal profiles are observed whenever similar fueling schemes are adopted for different divertor geometries. The explored shapes are shown in figure 9 where we discriminate the configurations dubbed as VT5C (Vertical-Horizontal target with OSP on Tile 5, Stack C), VT5D (Vertical-Horizontal target with OSP on Tile 5, Stack D) VV (Vertical-Vertical) and CC (Corner-Corner).

In panel (a) of Fig. 9 the separatrix density as a function of the applied gas rate for the different configurations experiments is reported. The mentioned differences among divertor geometries can be clearly recognized since different values of $n_{e,sep}$ are achieved with the same level of puffing. Such differences can be understood by considering that the variation of the Outer Strike Point (OSP) clearly modifies the closure of the divertor, the field line target angle and pump conductance which ultimately determine the recycling conditions as well the neutral pressure in the divertor region.

On the other side, as clearly highlighted in [26, 27], the OSP temperature represents the key physical ingredient to discriminate between the different divertor recycling states. The divertor outer target electron temperature is inferred from the Balmer photo-recombination continuum emission integrated along the LOS, as described in [28, 29]. The 17mm spatial resolution combined with fluctuations in the position of the strike point over the 40 ms camera integration time result in a somewhat smeared peak. Hence, we regard the temperature measurement at the OSP to be an average, $\langle T_{e,OT} \rangle$, in the proximity of the OSP. The above technique is well suited for analysis of the divertor target conditions in the outer horizontal (VT5) configuration due to the optimized divertor spectroscopy viewing geometry. This level of detail is not available for diagnosing the outer target parameters in the vertical (VV) and corner (CC) configurations due to the partially obstructed view and spectrometer chord incidence angle with the vertical target. $\langle T_{e,OT} \rangle$ in the VV configuration is estimated from the spectroscopy chord closest to the OSP, which is not terminated at the upper divertor tile. In CC configuration the OSP is not in view of the divertor spectroscopy chords. Even so, the outer most chord on tile 6 provides valuable information on the target electron temperature,

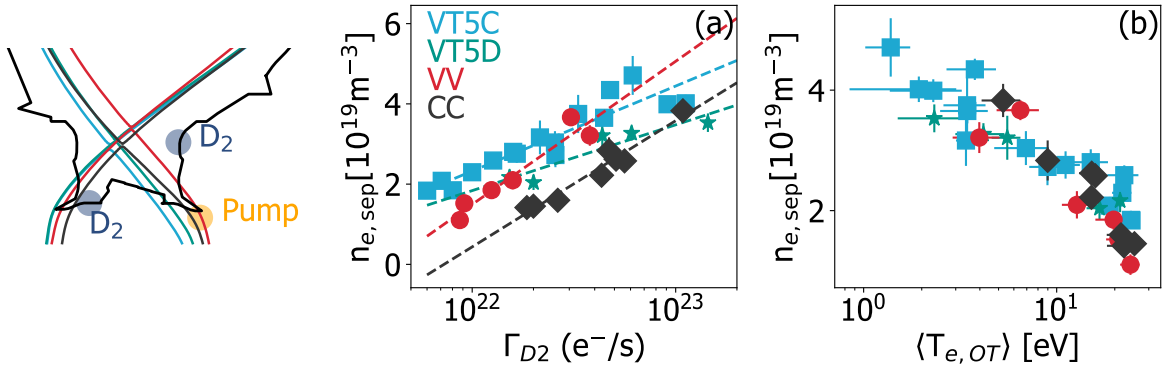

FIG. 9: Left panel: JET divertor with separatrix highlighted for the 4 configurations explored: Vertical Horizontal with OSP on the Tile 5 stack C (VT5C), Vertical-Horizontal with OSP on the Tile 5 Stack D (VT5D), Corner Corner configuration (CC), Vertical-Vertical configuration (VV) (a) $n_{e,sep}$ as a function of gas rate Γ_{D_2} for all the configurations explored (b) $n_{e,sep}$ as a function of spectroscopically determined average outer target temperature $\langle T_eOT\rangle$

and an empirical scaling factor has been derived to estimate $\langle T_{e,OT}\rangle$ in the corner configuration as described in [30]. The scaling of the separatrix density as a function of $\langle T_{e,OT}\rangle$ is shown in figure 9 (b): clearly this quantity is able to reconcile the differences among the configurations which collapse in an unified trend. To clarify how the $\langle T_{e,OT}\rangle$

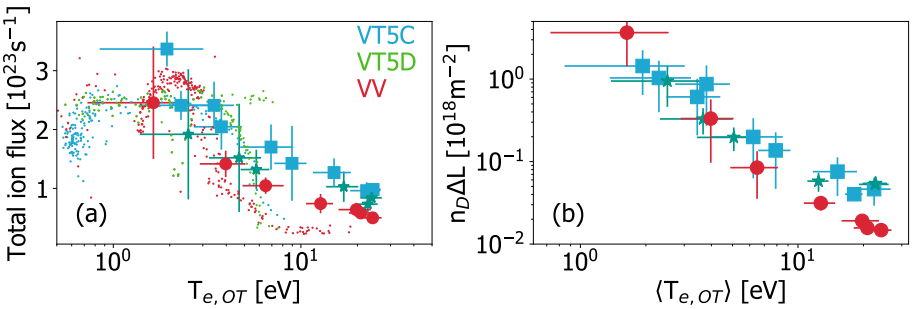

FIG. 10: (a) Total ion flux as a function of $\langle T_{e,OT}\rangle$. Small points indicate L-mode shots, symbols refer to inter-ELM H-mode plasmas and the colors distinguish the different divertor geometry (b) Line integrated neutral density as a function of $\langle T_{e,OT}\rangle$

relate to the recycling conditions we compute the total inter-ELM outer target ion flux from divertor langmuir probes as a function of divertor temperature. The outcome of this evaluation is shown in figure 10 (a). The smaller points represents the outer target total ion flux, with appropriate scaling, for L-mode density ramps where a clear roll-over is observed for target temperature $\langle T_{e,OT}\rangle \lesssim 2-3$ eV. We recognized that the H-mode investigation, shown for the different configuration in colored symbols, follow the same trajectory and that once considered as a function of $\langle T_{e,OT}\rangle$ all the configurations exhibit a similar trend with outer temperature target. Also we confirm that with this combination of power and injected gas no clear ion-flux rollover is observed and the divertor remains at most in high-recycling regime. In the same figure in panel (b) we provide an estimate of the quantity nDDL representing the product of the atomic neutral density and the effective emission path length. Such an estimated is based on the inverse photon efficiency (S/XB) method using absolutely calibrated radial D_α profiles in the outer divertor and ADAS S/XB coefficients constrained with spectroscopically derived ne and Te. Details of this measurement are described in [28]. A clear correlation is observed between this neutral density estimate and the outer target temperature, confirming that the $\langle T_{e,OT}\rangle$ ultimately characterize the divertor recycling state, neutral density and thus, similarly to what observed in AUG and JET the separatrix density. It is worth mentioning that, although the scenarios achieved high-recycling condition close to the outer target flux rollover, only ELM size reduction and ELM frequency increase are obtained, without any signature of transition to QCE regime. Nevertheless clear modification of the upstream profiles have been observed in all the geometries. As an example in Fig. 11 (a) we show the inter-ELM upstream profiles normalized to the separatrix values at two different values of $\langle T_{e,OT}\rangle$ in VV condition. A clear flattening of the density profile is observed differently to what reported in previous investigation [13]. In the same figure in panel (b) we provide an estimate of the density decay length λ_n as an average in the far SOL as a function of target temperature, or equivalently of divertor neutral pressure confirming the flattening of the profiles at higher neutral density. Concerning the fluctuations, we monitored the statistical properties of wall mounted probe in the inter-ELM phase. For this purpose we provide the scaling of the Skewness of the ion saturation current density J_s as a function of $\langle T_{e,OT}\rangle$ in Fig. 11 (c) with a clear increase of the skewness whenever higher-recycling is achieved, confirming the more intermittent behavior at higher neutral pressure and separatrix density observed for AUG and TCV

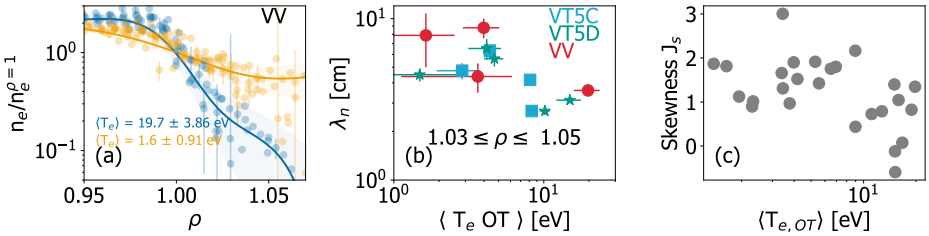

FIG. 11: (a) Upstream profiles normalized to the value at the separatrix in two different recycling conditions in VV divertor configuration (b) Density e-folding length in the far SOL as a function of $\langle T_{e,OT} \rangle$ for all the configuration explored (c) Ion saturation current skewness as measured from wall langmuir probe as a function of $\langle T_{e,OT} \rangle$

5 CONCLUSIONS

A cross-machine investigation of the effect of increasing fuelling on the separatrix and upstream SOL profiles has been performed, combining experiment on ASDEX-Upgrade, TCV and JET. Despite the differences in wall material, divertor closure and machine size we were able to identify some commonalities: in all the devices the neutral pressure achieved in the divertor region sets the separatrix density and collisionality. The change of collisionality implies a change in the turbulent parameter α_t whose increase can be considered as a signature of a more ballooning dominated turbulence close to the separatrix. At higher neutral pressure the inter-ELM H-Mode profiles tend to develop a flatter profile with an increase of the far SOL e-folding length. Both on AUG and TCV this is observed to occur together with a modification of the ELM stability and the appearance of the so-called QCE regime. On JET, shoulder appears even if no transition to QCE is observed. A strong enhancement of the SOL filaments activity is observed with the divertor neutral density and correspondingly α_t, with an increase of the filament frequency and, at least on AUG where measurements were available, with an increase of the radial velocity. All this combined observation suggests that the larger value of α_t achieved by the increase of separatrix density tightly linked to the increase of neutral pressure, cause an increase of convective transport which ultimately induce the appearance of a flatter SOL profile.

Acknowledgment

This work has been carried out within the framework of the EUROfusion Consortium and has received funding from the Euratom research and training programme 2014-2018 and 2019-2020 under grant agreement No 633053. The views and opinions expressed herein do not necessarily reflect those of the European Commission

REFERENCES

[1] R. Pitts et al., Nuclear Materials and Energy, 100696 (2019).
[2] N. Asakura et al., Journal of Nuclear Materials **241-243**, 559–563 (1997).
[3] B. LaBombard et al., Phys. Plasmas **8**, 2107 (2001).
[4] D. Carralero et al., Phys. Rev. Lett. **115**, 215002 (2015).
[5] F. Militello et al., Nucl. Fusion **56**, 016006 (2016).
[6] N. Vianello et al., Nucl. Fusion **57**, 116014 (2017).
[7] B. LaBombard et al., Journal of Nuclear Materials **241-243**, 149–166 (1997).
[8] J. A. Boedo et al., Physics of Plasmas **8**, 4826–4833 (2001).
[9] D. Carralero et al., Nucl. Fusion **57**, 056044 (2017).
[10] H. W. Müller et al., Journ of Nucl. Mater. **463**, 739–743 (2015).
[11] N. Vianello et al., Nuclear Fusion **60**, 016001 (2019).
[12] M. Faitsch et al., Nuclear Materials and Energy **26**, 100890 (2021).
[13] A. Wynn et al., Nuclear Fusion **58**, 056001 (2018).
[14] G. F. Harrer et al., Nuclear Fusion **58**, 112001 (2018).
[15] T. Eich et al., Nuclear Fusion **58**, 034001 (2018).
[16] T. Eich et al., Nuclear Fusion **60**, 056016 (2020).
[17] H. Reimerdes et al., Nuclear Fusion **61**, 024002 (2021).
[18] A. Kallenbach et al., Nuclear Materials and Energy **18**, 166–174 (2019).
[19] T. L. d. Cortemiglia et al., Nuclear Fusion (2020).
[20] B. N. Rogers et al., Physical Review Letters **81**, 4396–4399 (1998).
[21] D. Carralero et al., Nuclear Materials and Energy **12**, 1189–1193 (2017).
[22] M. Griener et al., Review of Scientific Instruments **89**, 10D102.
[23] C. Theiler et al., Nuclear Fusion **57**, 072008 (2017).
[24] P. Tamain et al., Journal of Nuclear Materials **463**, 450–454 (2015).
[25] E. Joffrin et al., Nuclear Fusion **57**, 086025 (2017).
[26] P. C. Stangeby, Plasma Physics and Controlled Fusion **60**, 044022 (2018).
[27] P. Stangeby, Plasma Physics and Controlled Fusion **62**, 025012 (2020).
[28] B. Lomanowski et al., Plasma Physics and Controlled Fusion **62**, 065006 (2020).
[29] B. Lomanowski et al., Nuclear Materials and Energy, 100676 (2019).
[30] B. A. Lomanowski et al., in preparation (2021).